Available online at www.sciencedirect.com
SCIENCE DIRECT
Journal of Power Sources 157 (2006) 136–152
JOURNAL OF POWER SOURCES
www.elsevier.com/locate/jpowsour

Effect of gas channel depth on current density distribution of polymer electrolyte fuel cell by numerical analysis including gas flow through gas diffusion layer

Gen Inoue *, Yosuke Matsukuma, Masaki Minemoto

Department of Chemical Engineering, Faculty of Engineering, Kyushu University, Hakozaki, Higashi-ku, Fukuoka 812-8581, Japan

Received 24 May 2005; received in revised form 5 August 2005; accepted 10 August 2005
Available online 15 September 2005

Abstract

In order to apply a numerical analysis to design an actual scale separator in polymer electrolyte fuel cell (PEFC), it is needed to enlarge the calculation size. In this study, mass transfer and flow in gas diffusion layer were calculated, and gas diffusion layer (GDL) mass transfer approximate model based on the theoretical model was developed. Next, with this model, PEFC reaction and thermal flow analysis model, which enabled us to calculate the case of an actual scale cell, was made. Furthermore, the effects of separator channel depth on output performance and current density distribution were examined with this numerical analysis. As a result, in the case of shallow channels, the oxygen transfer rate to electrode increased because of gas flow in GDL. However, current density distribution and pressure drop increased, too. This calculation model can help us to design the optimal separator shape from the comprehensive viewpoint.

Keywords: PEFC; Numerical analysis; Current density distribution; Gas diffusion layer; Pressure drop

1. Introduction

Recently, humankind has serious problems of the environment and energies, for example, global warming, acid rain or lack of fuel sources. In order to contribute to solve these problems, fuel cell is expected to be practical use because it has low emission of the environmental pollutant and high conversion efficiency from chemical energy to electrical energy. Especially, polymer electrolyte fuel cell (PEFC) is expected as driving power of vehicles and stationary power supply. And the performance of PEFC is greatly improved because of the development of new component and optimization of the system. However, PEFC is demanded to have long life and high durability to be generalized more widely as soon as possible. The PEFC power generation characteristic is affected by the structure, the material and operating conditions. The phenomena of mass transfer, heat transfer, catalysis, electrochemical reaction and fluid dynamics are shown in the internal cell, and it is greatly important to understand the correlation of such complex phenomena in detail to improve and optimize the PEFC component and system. However, regardless of the size of area from the interface of catalyst layer and the stack, these phenomena are caused. And these phenomena affect each other intricately. Therefore, it is very difficult to measure local condition accurately in experiments, and very few researchers examine these things.

Recently, a numerical analysis method has been used to examine them. Bernardi and Verbrugge [1,2] and Springer et al. [3] developed a one-dimensional model to the direction of membrane thickness, and examined concentration distribution and water management in PEFC. Fuller and Newman [4] developed a two-dimensional model to the direction of membrane thickness and gas flow channel. Nguyen and White [5] and Yi and Nguyen [6] developed heat and water transport models (2D) that accounted for various operation conditions and membrane hydration conditions. On the other hand, it is thought that analysis with the computational fluid

* Corresponding author. Tel.: +81 92 642 3523; fax: +81 92 642 3523.
E-mail address: ginoue@chem-eng.kyushu-u.ac.jp (G. Inoue).

0378-7753/$ – see front matter © 2005 Elsevier B.V. All rights reserved.
doi:10.1016/j.jpowsour.2005.08.004

Nomenclature

b_c	condensation rate constant (s^{-1})
C_j	molar concentration of species j (mol m^{-3})
$C_{j(n)}$	molar concentration of species j in next channel of n direction (mol m^{-3})
$C^e_{O_2}$	oxygen concentration at catalyst layer (mol m^{-3})
$C^{in}_{O_2}$	oxygen concentration at $x=0$ in Fig. 7 (mol m^{-3})
$C^{ref}_{O_2}$	reference oxygen concentration (mol m^{-3})
C_p	specific heat at constant pressure (J kg^{-1} K^{-1})
D_j	diffusion coefficient of species j (m^2 s^{-1})
D^{eff}_j	effective diffusion coefficient of species j (m^2 s^{-1})
erf	error function
E	electromotive force (V)
$E_{\Delta H}$	the value of reduction change of water enthalpy to voltage (V)
F	Faraday's constant (96,485 C mol^{-1})
h	heat transfer coefficient of gas (J m^{-2} s^{-1} K^{-1})
H_{GDL}	length of GDL gas flow area in Fig. 7 (m)
ΔH_{H_2O}	change of water enthalpy between vapor and liquid (J mol^{-1})
i	current density (A m^{-2})
i_{O_2}	oxygen exchange current density (A m^{-2})
k	thermal conductivity of solid phase (J m^{-1} s^{-1} K^{-1})
k_p	permeability of GDL (m^2)
k^{sep}	thermal conductivity of separator (J m^{-1} s^{-1} K^{-1})
$l_{d,g}$	gas channel depth (m)
l_{GDL}	GDL thickness (m)
l^s	thickness of solid phase (m)
l^{sep}	separator thickness between back plate and gas phase (m)
M_j	molecular weight of species j (kg mol^{-1})
$N^e_{O_2(reaction)}$	oxygen reaction rate at electrode (mol m^{-2} s^{-1})
$N^e_{O_2(Re)}$	increased oxygen mole flux to electrode by gas flow (mol m^{-2} s^{-1})
$N^e_{O_2(Re=0)}$	oxygen mole flux to electrode at $Re=0$ (mol m^{-2} s^{-1})
p	pressure in Eqs. (2), (3), (28) and (36) (Pa)
p_n	pressure in next channel of n direction (Pa)
$P_{H_2O,sat}$	saturated vapor pressure in stream (Pa)
Pe	Peclet number defined in Eq. (23)
q_1	heat flux from solid phase to gas phase (J m^{-2} s^{-1})
q_2	heat flux from back plate to gas phase (J m^{-2} s^{-1})
q_3	heat value generated by reaction (J m^{-2} s^{-1})
q_4	heat flux from gas phase to solid phase (J m^{-2} s^{-1})
q_5	heat flux from back plate to solid phase (J m^{-2} s^{-1})
q_6	latent heat value of condensation (J m^{-2} s^{-1})
Q_b	all gas flow rate through GDL per unit volume to next channel (s^{-1})
$Q_{b(n)}$	flow rate through GDL per unit volume to next channel of n direction (s^{-1})
$Q_{b(n,in)}$	inflow rate through GDL per unit volume from next channel of n direction (s^{-1})
$Q_{b(n,out)}$	outflow rate through GDL per unit volume to next channel of n direction (s^{-1})
r_j	molar flux of species j (mol m^{-2} s^{-1})
R	gas constant (8.314 J mol^{-1} K^{-1})
R_{ohm}	resistance of proton transfer through electrolyte membrane (Ω m^2)
R_{rea}	all reaction rate (s^{-1})
Re	Reynolds number defined in Eq. (8)
Sc	Schmidt number defined in Eq. (9)
Sh	Sherwood number defined in Eq. (20)
t	time (s)
T	gas phase temperature (K)
T_n	gas temperature in next channel of n direction (K)
T^s	solid phase temperature (K)
T^b	back plate temperature (K)
U	average gas velocity in GDL of x direction (m s^{-1})
U_T	overall heat transfer coefficient between gas and back plate (J m^{-2} s^{-1} K^{-1})
U^s_T	overall heat transfer coefficient between back plate and solid phase (J m^{-2} s^{-1} K^{-1})
v	flow velocity (m s^{-1})
V	operation voltage (V)
w_C	channel width (m)
w_L	land width (m)
x	distance in x direction (m)
y	distance in y direction (m)

Greek letters

α	net water transfer coefficient
α_t	transfer coefficient
β	fitting parameter defined in Eq. (11)
ε	effective porosity of GDL
γ	variable defined in Eq. (7) (A m mol^{-1})
λ	parameter defined in Eq. (21)
μ	viscosity of mixture gas (Pa s^1)
ρ	density of mixture gas (kg m^{-3})

Superscripts

a	anode
c	cathode

channel	channel
e	electrode
eff	effective
k	anode or cathode
s	solid phase
sep	separator

Subscripts

ave	average
H_2O	water
H_2O(l)	liquid water
H_2O(v)	vapor water
j	species *j*
N_2	nitrogen
O_2	oxygen
x	*x* direction
y	*y* direction

dynamics (CFD) technique is important to calculate the transport phenomena in detail, and studies of this kind have been increasing recently. Um et al. [7] and Wang et al. [8] developed the two-dimensional model with CFD, which included two-phase flow. Dutta et al. [9] made a three-dimensional computational model based on a commercial software package (Fluent). Berning et al. [10] presented a non-isothermal and the three-dimensional models, and calculated the distribution of current density and concentration in straight channels. Mazumder and Cole [11] examined the liquid water transport with the three-dimensional model. Li et al. [12] analyzed the flow and concentration distribution in a small cell with the three-dimensional analysis. Berning and Djilali [13] examined the effect of porosity and thickness of gas diffusion layer in straight channels with the three-dimensional model. These PEFC numerical analysis models contributed to the optimization of component design and operation conditions, and the examination of issues included in the present cell.

In PEFC, anode and cathode gases usually flow through each channel. And the reactant gas diffused to the interface of membrane electrode assembly (MEA) through gas diffusion layer (GDL). GDL is porous, and it plays a role to help hydrogen and oxygen move to an electrode catalyst, to support MEA and to pass the electron. The ordinary gas flow situation is shown in Fig. 1. However, in the case of a large-scale cell, it is thought that the differential pressure between adjoining channels increases, and that the supplied gas flows through GDL owing to the differential pressure. This is shown in Fig. 2. As a result, it is supposed that the cell endurance decreases because the temperature and the humidity condition are not uniform. However, it can be expected that oxygen transfer rate to electrode and output density increase by such gas flow in GDL. Therefore, it is important to examine the influence of this gas flow on cell

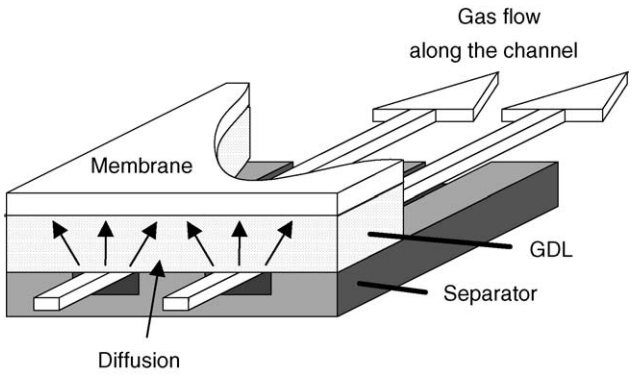

Fig. 1. Ordinary gas flow condition in PEFC.

performance and to optimize operating condition and cell shape.

Nguyen [14] proposed the interdigitated channel that had the closed channel, and supplied gas was forced to flow through GDL. Um and Wang [15] examined gas flow in this interdigitated channel with two phases and the three-dimensional model. But, in the case of a large-scale cell, there was a possibility that such gas flow through GDL was occurred by large pressure drop in usual channel shape. Dohle et al. [16] and Oosthuizen et al. [17] mentioned this gas flow through GDL with serpentine channel and examined gas flow rate distribution experimentally and numerically. But current density distribution and cell performance were not examined.

In our past researches [18], the effects of changing operation temperature, humidify temperature and hydrogen and oxygen concentration in supply gas on the *i–V* characteristic of a small PEFC were examined experimentally. For the experiment, we developed two models: one was PEFC reaction model that could show these influences on PEFC reaction characteristics, and the other was PEFC reaction and flow analysis model that was combined with the thermal flow analysis. With this PEFC reaction and flow analysis model, five kinds of separators were evaluated from the viewpoint as follows: gas flow condition, uniformity of current density and temperature, reduction of pressure drop and ejection of water. In [19], the simplified two-dimensional PEFC analysis

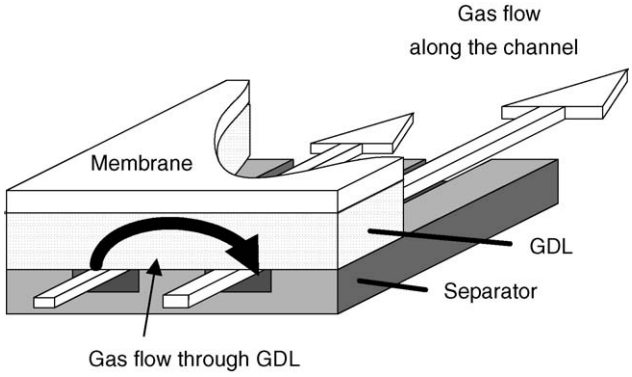

Fig. 2. Gas flow through gas diffusion layer.

model including flow and heat transfer of cooling water was made. And the influence of changing thickness of membrane and GDL on cell performance was calculated. However, these our past models did not include the effect of gas flow through gas diffusion layer. As the gas flow rate and concentration and temperature are not uniform in an actual cell, it is also important to examine the effect of internal phenomena on cell performance in an actual-sized cell with an area of 10 cm^2. This examination enables to identify the factors which influence cell output performance and durability, and to optimize the PEFC system. In this study, especially gas flow through GDL was aimed, and our former analysis model was improved. The effect of gas flow through GDL on the cell performance and internal phenomena of an actual PEFC single cell was examined. As mentioned above, in other studies which examined concentration and liquid water distribution in GDL by a numerical analysis including gas flow through GDL, the strict analysis model based on CFD with an area of several square millimeters was mainly used. Therefore, from the viewpoint of calculation resources and calculation time, it is difficult to extend this former model, which was used in other studies to an actual-sized cell. In this study, the numerical analysis model was separated two models in consideration of practical calculation resources and practical calculation time. First, two-dimensional mass transfer and flow in cathode GDL were calculated, and the effect of gas flow through GDL on oxygen mass transfer rate to electrode was examined under various conditions. This results and theoretical mass transfer model were combined, and the approximate model of oxygen mass transfer in cathode GDL was developed. Second, with this model, the quasi-two-dimensional PEFC reaction and thermal flow analysis model, which enabled to calculate an actual-sized cell was made. Furthermore, the effect of separator channel depth on output performance and current density distribution was examined by this numerical analysis including gas flow though GDL.

2. Numerical analysis model including gas flow through GDL

In this study, the PEFC numerical analysis model was developed step by step. First, equations of motion and mass balance in gas diffusion layer were calculated by the finite difference method. And GDL mass transfer approximate model including the effect of gas flow through GDL was made. Next, with this approximate model, PEFC reaction and thermal flow analysis model, which could calculate an actual scale cell, was developed.

2.1. Mass transfer and flow analysis in GDL and development of approximate model

PEFC consists of MEA, two GDLs and two separators. Polymer membrane of MEA has proton conductivity and is sandwiched between two thin platinum electrode layers. MEA is sandwiched between two GDLs and two separators. In this study, it was assumed that hydrogen transfer rate in anode GDL was faster than the other mass transfer rate and reaction rate in PEFC, and only oxygen transfer in cathode GDL was examined. Fig. 3 shows a schematic of mass transfer and flow analysis in cathode GDL. Thickness of GDL (l_{GDL}) was 300 μm, and width of channel (w_C) and land (w_L) were both 1 mm. The governing equations in this simulation were derived from the following assumptions:

1. The effective porosity and the permeability were uniform in GDL.
2. Water condensation was ignored in GDL.
3. Density, viscosity and diffusion coefficient of cathode gas were not uniform actually because the composition was changed locally. However, in this study, these values were regarded as constant and uniform for convenience.
4. Electrolyte membrane was humidified well, and ionic conductivity was constant and uniform.
5. Water transfer and gas crossover through membrane were ignored.
6. Gas flow condition in GDL was laminar flow.
7. Cell voltage was uniform.
8. The difference of concentration between adjoining channels was very little, and the concentration of channels was set to be equal to each other.

The equation of continuity is shown by the following expression:

$$\frac{\partial \rho v_x}{\partial x} + \frac{\partial \rho v_y}{\partial y} = 0 \tag{1}$$

where ρ is density of mixed gas and v_x and v_y are velocity of x and y directions.

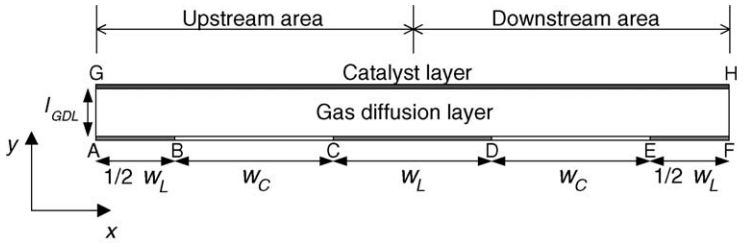

Fig. 3. Calculation model of cathode gas diffusion layer in PEFC.

The equation of motion in gas diffusion layer, which was porous media, was derived from Darcy's model.

$$v_x = -\frac{k_p}{\mu}\frac{\partial p}{\partial x} \tag{2}$$

$$v_y = -\frac{k_p}{\mu}\frac{\partial p}{\partial y} \tag{3}$$

where k_p is the permeability of GDL, μ the viscosity of mixed gas and p is the pressure.

The equation of mass balance of cathode gas is shown by the following expression:

$$0 = -\frac{\partial}{\partial x}(C_j v_x) - \frac{\partial}{\partial y}(C_j v_y) + D_j^{\text{eff}}\frac{\partial^2 C_j}{\partial x^2} + D_j^{\text{eff}}\frac{\partial^2 C_j}{\partial y^2} \tag{4}$$

where C_j is the concentration of chemical species j and D_j^{eff} is the effective diffusion coefficient of j. This equation was derived to oxygen, vapor and nitrogen. The effective diffusion coefficient was calculated with effective porosity by the following equation:

$$D_j^{\text{eff}} = \varepsilon D_j \tag{5}$$

In this study, overvoltage of anode reaction was ignored, and the relationship between cell voltage and overvoltage is shown by the following equation:

$$V = E - \frac{RT}{\alpha_t 2F}\ln\left[\frac{iC_{O_2}^{\text{ref}}}{i_{O_2}C_{O_2}^{\text{e}}}\right] - R_{\text{ohm}}i \tag{6}$$

where E is electromotive force, R the gas constant, T the temperature, α_t the transfer coefficient, F the Faraday's constant, i the current density, i_{O_2} the exchange current density, $C_{O_2}^{\text{ref}}$ the reference oxygen concentration, $C_{O_2}^{\text{e}}$ the oxygen concentration at an interface of catalyst layer and R_{ohm} is resistance of proton transfer through the electrolyte membrane. R_{ohm} was calculated by Nguyen's equation [5]. Reference oxygen concentration and exchange current density in Eq. (6) were shown as the variable γ by the following equation:

$$\gamma = \frac{i_{O_2}}{C_{O_2}^{\text{ref}}} \tag{7}$$

In order to calculate Eqs. (1)–(6), boundary conditions were given by the following equations:

(Face A–B, C–D and E–F)

$$\frac{\partial p}{\partial y} = 0, \qquad \frac{\partial C_{O_2}}{\partial y} = \frac{\partial C_{H_2O}}{\partial y} = \frac{\partial C_{N_2}}{\partial y} = 0$$

(Face B–C and D–E)

$$p_{BC} = p_{\text{in}}, \quad p_{DE} = p_{\text{out}} \qquad C_{O_2} = C_{O_2}^{\text{channel}},$$
$$C_{H_2O} = C_{H_2O}^{\text{channel}}, \quad C_{N_2} = C_{N_2}^{\text{channel}}$$

Table 1
Calculation condition of GDL mass transfer analysis

Differential pressure between channels (Pa)	0–1000
Temperature (°C)	60
Transfer coefficient	0.3
Effective porosity	0.1–0.3
Cathode gas density (kg m^{-3})	0.977
Cathode gas viscosity (Pa s)	1.81×10^{-5}
Permeability of GDL (m^2)	2.50×10^{-11}
Electromotive force (V)	1.23
Membrane thickness (μm)	30
Oxygen diffusion coefficient (m^2 s^{-1})	2.00×10^{-5}
γ of Eq. (7) (A m mol^{-1})	4.0×10^{-2}

(Face G–H)

$$\frac{\partial p}{\partial y} = \frac{\mu}{k_p}\frac{-i}{4F\rho}\left[M_{O_2} - 2M_{H_2O}\right] \qquad \frac{\partial C_{O_2}}{\partial y} = \frac{i}{4FD_{O_2}^{\text{eff}}},$$
$$\frac{\partial C_{H_2O}}{\partial y} = -\frac{i}{2FD_{H_2O}^{\text{eff}}}, \qquad \frac{\partial C_{N_2}}{\partial y} = 0$$

(Face A–G and F–H)

$$\frac{\partial p}{\partial x} = 0,$$

C_j is periodic boundary condition between A–G and F–H

It is necessary to note that the analysis model of mass transfer and flow in GDL was developed as a local model for making the approximate model of oxygen mass transfer in cathode GDL, and that it was not developed for the examination of the whole actual cell. In this study, it was assumed that periodic boundary condition was applied on the right and left sides of GDL (Face A–G and F–H) in Fig. 3, though it is not appropriate in consideration of the actual cell realistically.

Eqs. (1)–(6) were calculated with above boundary condition by the finite difference method. Calculation condition was shown in Table 1. In this study, the effect of liquid water was not directly included in this analysis model, in other words, the equations of motion and mass balance of liquid water were not calculated. So the effect of diffusion inhibition of liquid water in GDL cannot be directly evaluated. However, in this model, GDL effective porosity was used as one parameter when the oxygen mass transfer rate in GDL was calculated. This value was different from real GDL porosity, and it was used as apparent GDL porosity including liquid water. So GDL effective porosity was assumed as 0.1–0.3 to include the effect of liquid water in GDL for convenience, though real GDL porosity was about 0.70. In this study, current density and oxygen concentration distribution were examined with this analysis model changing differential pressure and effective porosity. And in order to estimate the effect of flow, dimensionless numbers were defined by the following equations:

$$Re = \frac{l_{\text{GDL}}\rho U}{\mu} \tag{8}$$

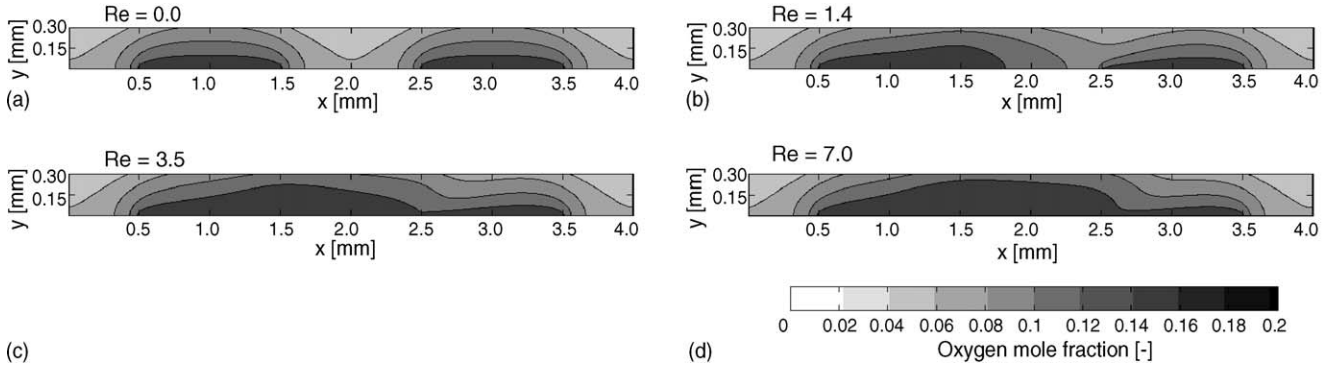

Fig. 4. (a–d) Oxygen mole fraction distribution in GDL at 0.6 V: effective porosity is 0.3.

$$Sc = \frac{\mu}{\rho D_{O_2}^{\text{eff}}} \tag{9}$$

Re is the Reynolds number, *U* the average velocity of the *x* direction at $x = 2$ mm and *Sc* is the Schmidt number.

Figs. 4 and 5 show oxygen mole fraction distribution at 0.6 V and 0.5 V, respectively. In these graphs, in the case of (a) $Re = 0.0$, which differential pressure between channels was almost zero and gas did not flow, it was found that oxygen moved to the upper area of the channel section more than that of the land section. And comparing Figs. 4 and 5, oxygen concentration distribution became large with low cell voltage. Next, changing the differential pressure between channels, it was found that oxygen moved to the upper area of the land section by gas flow, and that the effect became large according to Reynolds number in Figs. 4b–d and 5b–d. Fig. 6 shows current density distribution at 0.6 V. As gas flow velocity was large, current density was high at the upper area of the land section. On the other hand, current density at the upper area of a downstream channel ($x = 2.0$–4.0 mm) was affected by convection flowing out to the downstream channel, and it was locally lower than that without gas flow. Moreover, when *Re* was 0.0, 1.4, 3.5 and 7.0, the average current densities were 0.862, 0.884, 0.900 and 0.911 A cm^{-2}, respectively, and it was found that the average current density was not proportional to the Reynolds number. At face A–G and F–H, the periodic boundary condition was applied. However in this calculation results, the concentration gradient at this boundary was almost zero, and the mass flux through this boundary by diffusion could be ignored. In other words, the calculation results equaled to the results with the boundary condition that concentration gradient was zero, and this boundary condition did not affect the whole calculation results.

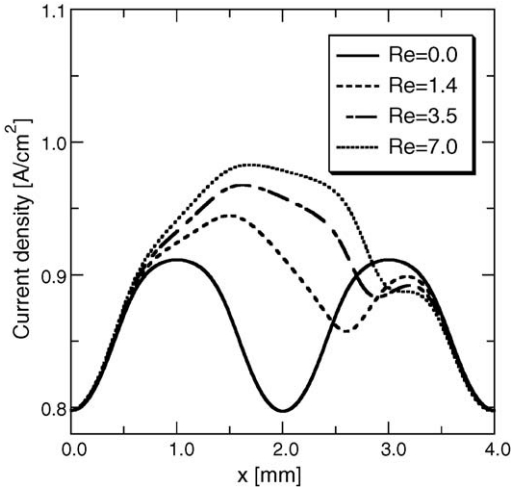

Fig. 6. The effect of gas flow through GDL on current density distribution at 0.6 V: effective porosity is 0.3.

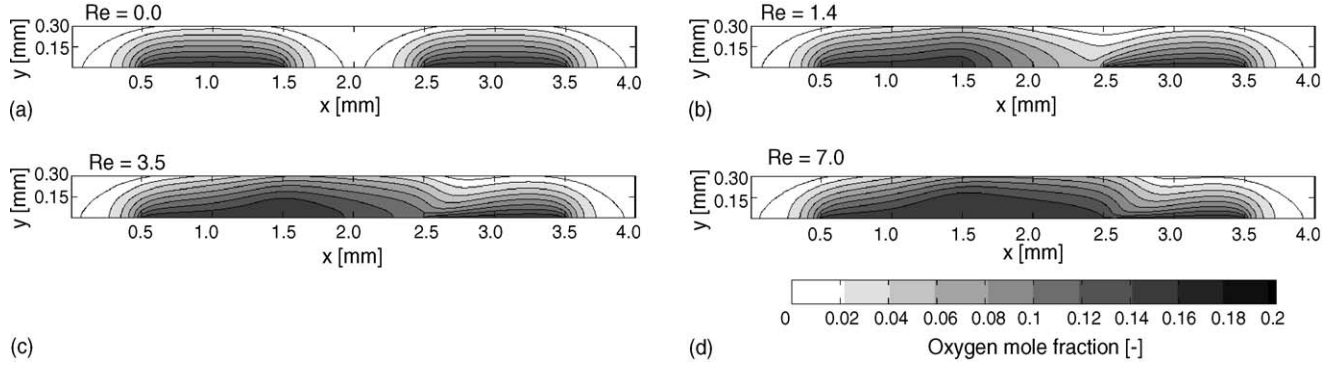

Fig. 5. (a–d) Oxygen mole fraction distribution in GDL at 0.5 V: effective porosity is 0.3.

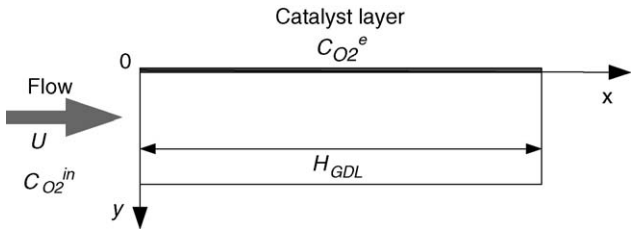

Fig. 7. Schematic of GDL approximate model.

Mass transfer with gas flow was examined by the numerical analysis mentioned above. However, it was difficult to apply this model to an actual scale cell from the viewpoint of calculation time and calculation resource. So the simplified mass transfer model, which expressed oxygen transfer with gas flow through GDL, was developed. In this study, it was based on a theoretical model, and given by fitting with numerical simulations. In Figs. 4 and 5, the section from $x=0$ mm to 2 mm was defined as an upstream area, and the section from $x=2$ mm to 4 mm was defined as a downstream area. The upstream area and the downstream area were decided by the direction of gas flow through GDL in this study, and these were not decided by the position of channels. And current density and oxygen concentration at catalyst layer were averaged in each section with 2 mm width. The rate of oxygen consumption by electrode reaction was equal to the summation of oxygen flux to catalyst layer without gas flow and oxygen flux by gas flow through GDL. This relationship is shown by the following equation:

$$N^{\mathrm{e}}_{\mathrm{O}_2(\mathrm{reaction})} = \frac{i}{4F} = N^{\mathrm{e}}_{\mathrm{O}_2(Re=0)} + N^{\mathrm{e}}_{\mathrm{O}_2(Re)} \tag{10}$$

These oxygen fluxes were modeled, respectively.

First, oxygen flux without gas flow was calculated by the following equation:

$$N^{\mathrm{e}}_{\mathrm{O}_2(Re=0)} = D^{\mathrm{eff}}_{\mathrm{O}_2} \frac{C^{\mathrm{channel}}_{\mathrm{O}_2} - C^{\mathrm{e}}_{\mathrm{O}_2}}{l_{\mathrm{GDL}}} \times \beta \tag{11}$$

where β is the fitting parameter and it is function of channel and GDL shape.

Next, oxygen flux with gas flow was examined. Fig. 7 shows the objective area to develop the theoretical model. In this figure, gas flowed to the x direction along the catalyst layer, but the y direction needs to be paid attention to because it is different from that in Fig. 3. The governing equations in this model were derived from the following assumptions:

1. Gas flow to the y direction is ignored.
2. Gas diffusion to the x direction is ignored.
3. Gas flow velocity is uniform in the y direction.
4. Oxygen concentration at $x=0$ is constant and uniform.
5. Oxygen concentration at interface of catalyst layer ($y=0$) is uniform.

The following convectional diffusion equation was derived from a mass balance equation of oxygen with above assumption:

$$U\frac{\partial C_{\mathrm{O}_2}}{\partial x} = D^{\mathrm{eff}}_{\mathrm{O}_2}\frac{\partial^2 C_{\mathrm{O}_2}}{\partial y^2} \tag{12}$$

And boundary conditions were shown by the following equation:

$$C_{\mathrm{O}_2} = C^{\mathrm{in}}_{\mathrm{O}_2}, \quad \text{at } x=0,\ y>0$$
$$C_{\mathrm{O}_2} = C^{\mathrm{e}}_{\mathrm{O}_2}, \quad \text{at } x>0,\ y=0$$

For the purpose of getting exact solution of Eq. (12) with above boundary condition, mathematical technique was required. The detailed solving method about this partial differential equation was described in other text, for example reference [20]. In this paper, the derivation of solution was omitted, and the following solution was obtained:

$$\frac{C^{\mathrm{e}}_{\mathrm{O}_2} - C_{\mathrm{O}_2}}{C^{\mathrm{e}}_{\mathrm{O}_2} - C^{\mathrm{in}}_{\mathrm{O}_2}} = \mathrm{erf}\left(\frac{y\sqrt{U}}{2\sqrt{D^{\mathrm{eff}}_{\mathrm{O}_2}x}}\right) \tag{13}$$

where erf is error function, and it is calculated by the following equation:

$$\mathrm{erf}(x) = \frac{2}{\sqrt{\pi}}\int_0^x \mathrm{e}^{-z^2}\,\mathrm{d}z \tag{14}$$

The oxygen mole flux at interface of catalyst layer was calculated by the following equation:

$$N^{\mathrm{e}}_{\mathrm{O}_2} = D^{\mathrm{eff}}_{\mathrm{O}_2}\left(\frac{\partial C_{\mathrm{O}_2}}{\partial y}\right)\bigg|_{y=0} \tag{15}$$

Eq. (16) was obtained by substituting Eq. (13) for Eq. (15)

$$N^{\mathrm{e}}_{\mathrm{O}_2} = (C^{\mathrm{in}}_{\mathrm{O}_2} - C^{\mathrm{e}}_{\mathrm{O}_2})\sqrt{\frac{D^{\mathrm{eff}}_{\mathrm{O}_2}U}{\pi x}} \tag{16}$$

The average oxygen mole flux of section H_{GDL} in Fig. 7 was obtained by integrating Eq. (16).

$$N^{\mathrm{e}}_{\mathrm{O}_2(\mathrm{ave})} = \frac{1}{H_{\mathrm{GDL}}}\int_0^{H_{\mathrm{GDL}}} N^{\mathrm{e}}_{\mathrm{O}_2}\,\mathrm{d}x = 2\sqrt{\frac{UD^{\mathrm{eff}}_{\mathrm{O}_2}}{\pi H_{\mathrm{GDL}}}}(C^{\mathrm{in}}_{\mathrm{O}_2} - C^{\mathrm{e}}_{\mathrm{O}_2}) \tag{17}$$

This average oxygen flux expresses the effect of gas flow through GDL. In this study, H_{GDL} was 4 mm, and this increased oxygen flux was divided into an upstream area and a downstream area. And it was assumed that $C^{\mathrm{in}}_{\mathrm{O}_2}$ was equal to the average of $C^{\mathrm{e}}_{\mathrm{O}_2}$ and $C^{\mathrm{channel}}_{\mathrm{O}_2}$.

$$N^{\mathrm{e}}_{\mathrm{O}_2(Re)} = \frac{1}{2}\sqrt{\frac{UD^{\mathrm{eff}}_{\mathrm{O}_2}}{\pi H_{\mathrm{GDL}}}}(C^{\mathrm{channel}}_{\mathrm{O}_2} - C^{\mathrm{e}}_{\mathrm{O}_2}) \tag{18}$$

With Eqs. (10), (11) and (18), the following equation was obtained:

$$\frac{i}{4F} = D_{O_2}^{\text{eff}} \frac{C_{O_2}^{\text{channel}} - C_{O_2}^{\text{e}}}{l_{\text{GDL}}} \times \beta + \frac{1}{2}\sqrt{\frac{UD_{O_2}^{\text{eff}}}{\pi H_{\text{GDL}}}}(C_{O_2}^{\text{channel}} - C_{O_2}^{\text{e}}) \quad (19)$$

The Sherwood number was defined by the following equation as a dimensionless number, which expressed mass transfer rate:

$$Sh = \frac{i}{4F} \frac{l_{\text{GDL}}}{D_{O_2}^{\text{eff}}(C_{O_2}^{\text{channel}} - C_{O_2}^{\text{e}})} \quad (20)$$

And the variable λ was defined by the following equation:

$$\lambda = \frac{1}{2}\sqrt{\frac{l_{\text{GDL}}}{\pi H_{\text{GDL}}}} \quad (21)$$

Eq. (19) was transformed with Eqs. (20) and (21)

$$Sh = \beta + \lambda\sqrt{Pe} = \beta + \lambda\sqrt{Re}\sqrt{Sc} \quad (22)$$

where *Pe* is the Peclet number, and it was calculated by the following equation:

$$Pe = \frac{Ul_{\text{GDL}}}{D_{O_2}^{\text{eff}}} = \frac{Ul_{\text{GDL}}\rho}{\mu}\frac{\mu}{\rho D_{O_2}^{\text{eff}}} = Re \cdot Sc \quad (23)$$

Eq. (22) is a simplified mass transfer model. In order to determine the fitting parameter β and to confirm the validity of this equation, the relationship between *Sh* and *Pe* (or *Re* and *Sc*) was examined by the numerical analysis as Eqs. (1)–(7). The average current density (*i*) and the average of difference of oxygen concentration ($C_{O_2}^{\text{channel}} - C_{O_2}^{\text{e}}$) between the upstream area and the downstream area were calculated by changing cell voltage from 0.9 to 0.05 with Eqs. (1)–(7) analysis. *Sh* was obtained from the gradient of those two quantities with Eq. (20). Moreover, calculations of such kind were repeated by changing differential pressure between channels and by changing effective porosity.

Fig. 8 shows the relationship between *Sh* and *Sc* at *Re* = 0 (differential pressure was zero). It shows *Sh* is independent of *Sc* and this value is about 0.624. From Eq. (22), it was confirmed that the value of β was 0.624. Fig. 9 shows the relationship between the Sherwood number and the Reynolds number. *Sh* increased greatly by *Re* in case of large *Sc*, and the mass transfer rate of an upstream area was affected more strongly than that of a downstream area by *Re*. *Sh* of the downstream area was not changed until *Re* came to the average 1.3 in each *Sc*, so the quantity that 1.3 subtracted from *Re* was used to examine Eq. (22). Fig. 10 shows the relationship between *Sh* and *Re*·*Sc* (=*Pc*) of the upstream area (a and b) and the downstream area (c). In Fig. 10a, a horizontal axis is *Re*·*Sc*, and a vertical axis is $(Sh - \beta)/\lambda$. If Eq. (22) is correct, all data are expressed by a solid line. But these data were not located on this line. Therefore, this equation

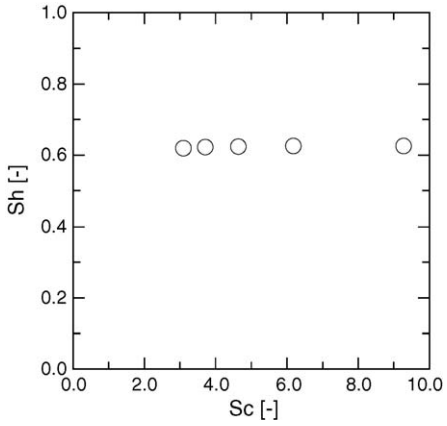

Fig. 8. Relationship between Sherwood number and Schmidt number: Reynolds number is zero.

was tried to prove it correct. In Fig. 10b, the vertical axis shows $(Sh - \beta)/(\lambda Sc^{0.3})$. In this graph, all data are shown by a solid line. It needs to correct for the following reasons. Eq. (22) was derived from the assumption of perfect parallel flow along the catalyst layer. But there was not such flow condition in the numerical simulation, and especially at the upstream area, oxygen in a gas channel was moved to a catalyst layer by vertical gas flow. Next in Fig. 10c, in the case of the downstream area, the equation of *Sh* could be modeled by $(Re - 1.3)$ in Eq. (22). Consequently, the simplified mass transfer model as followings were obtained by the theoretical models and the numerical simulations:

$$\begin{aligned} &\text{Upstream} && Sh = 0.624 + \lambda Re^{0.5} Sc^{0.8} && \\ &\text{Downstream} && Sh = 0.624 && Re < 1.3 \\ & && Sh = 0.624 + \lambda(Re - 1.3)^{0.5} Sc^{0.5} && Re > 1.3 \end{aligned} \quad (24)$$

Similar examinations were carried out as to the different oxygen concentration in gas channel and ionic conductivity of electrolyte membrane, and it was confirmed that the same equation was obtained from these examinations. The oxygen concentration at an interface of catalyst layer could be cal-

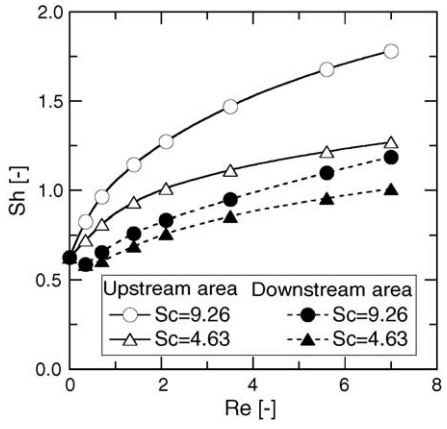

Fig. 9. Relationship between Sherwood number and Reynolds number.

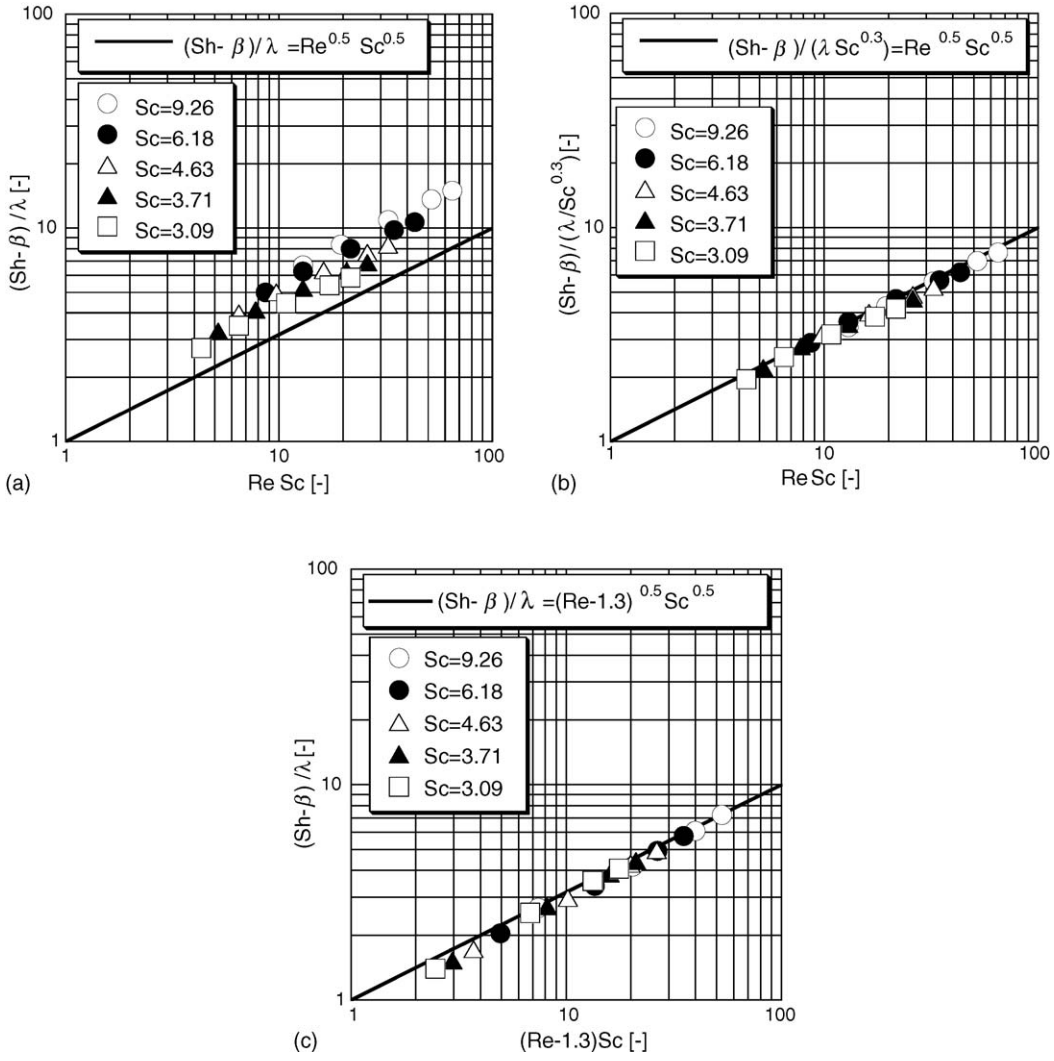

Fig. 10. Relationship between Sherwood number and Reynolds number·Schmidt number: (a) upstream area; (b) upstream area with correction; (c) downstream area.

culated with Eq. (24), and the characteristic of cell voltage and current density was calculated by substituting it for Eq. (6). But this model was given from the assumption that liquid water was ignored, it has to be improved in detail. As the numerical value in Eq. (24) was obtained with the shape of Fig. 3, these values were needed to examine in the case of other shapes, which meant different channel width, land width and thickness of GDL. However, in this study, the influence of cell shape on these values was not examined, and the calculation of the following section was carried out with the same shape.

2.2. PEFC reaction and thermal flow analysis model

The oxygen transfer model was developed in the previous section. In this section, the PEFC reaction and thermal flow analysis model, which could calculate an actual scale cell, was developed. As the definition of coordinate was different from that of previous section, and that is an important point to notice. Fig. 11 shows the PEFC simulation model. As shown in this figure, gas flow velocity, concentration and temperature were calculated in gas channels on the anode and the cathode. And it was assumed that the temperature distributions of MEA and GDL were the same as each other and they were unified, and the temperature and current density were calculated in the unified part. (This unified part is expressed as a solid phase.) The governing equations in this simulation were derived from the following assumptions:

1. The inlet gas flow rate in each channel is uniform.
2. The volume of the condensation water is ignored, and the water moves with the gas.
3. Reduction of the reaction area caused by flooding of electrode is ignored, and it is also ignored that water condensation prevents the diffusion.
4. Fluid is incompressible Newtonian fluid and ideal gas. Flow condition is laminar flow. Gas properties are constant.

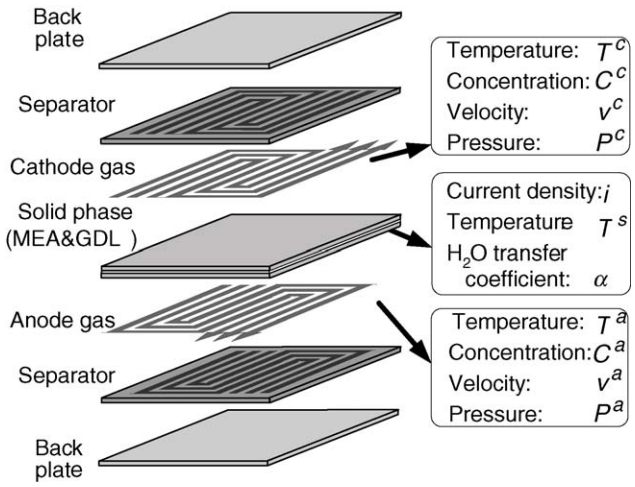

Fig. 11. Model for the simulation of the PEFC.

5. The temperature of back plate is uniform and constant.
6. Heat transfer between a separator and gas is ignored. But heat transfer among gas phase, solid phase and back plate is included.
7. Cell voltage is uniform and constant.
8. Only resistance overvoltage and water transfer in a membrane include the influence of temperature.
9. In a membrane, ionic conductivity, electro-osmosis coefficient and water effective diffusion coefficient that depend on the membrane humidity are determined by water activity of the anode side.
10. The gas crossover through a membrane is disregarded.
11. The permeability of GDL is constant and uniform.

In this study, the one-dimensional analysis as plug flow in each channel was available because of the assumption that the inlet gas flow rate distribution was uniform. Though the separator shape was a two-dimension structure to the direction of the membrane faces, the quasi-two-dimension analysis model was made by assuming the direction from the inlet to the outlet to be a positive x direction in each channel and by making a channel meander. As a result, simplification of the equations and reduction in calculation time became possible. However, in the case of calculation of the solid phase temperature distribution, it was calculated by the two-dimensional analysis model. And in order to calculate gas flow rate that flowed to the next channel through GDL, pressure distribution was calculated by the two-dimensional analysis. Moreover, for simplification of the calculation, these following two terms in gas channel were ignored: the heat conduction term in the energy balance equations; and the diffusion term in the mass balance equations.

The equation of continuity is shown by the following equation:

$$\frac{\partial v^{\mathrm{k}}}{\partial x} = -R^{\mathrm{k}}_{\mathrm{rea}} - Q^{\mathrm{k}}_{\mathrm{b}} \tag{25}$$

where v is the velocity of mixed gas, x the distance along a gas flow channel, R_{rea} the all reaction rate, Q_{b} the all gas flow rate through GDL per unit volume to the next channel and the superscript k is the anode side or the cathode side. R_{rea} is calculated by the following equation:

$$R^{\mathrm{k}}_{\mathrm{rea}} = \frac{1}{l^{\mathrm{k}}_{\mathrm{d,g}}\rho^{\mathrm{k}}}\sum_j M_j r^{\mathrm{k}}_j \tag{26}$$

where $l_{\mathrm{d,g}}$ is depth of gas channel, ρ the density of mixed gas, M_j the molecular weight of a chemical species j and r_j is the reaction or condensation rate per unit area of chemical species j. Q_{b} is calculated by the following equation:

$$Q^{\mathrm{k}}_{\mathrm{b}} = \sum_n Q^{\mathrm{k}}_{\mathrm{b}(n)} \tag{27}$$

where $Q^{\mathrm{k}}_{\mathrm{b}(n)}$ is gas flow rate through GDL to the n direction.

The equation of motion is shown by the following equation:

$$\rho^{\mathrm{k}}\frac{\mathrm{D}v^{\mathrm{k}}}{\mathrm{D}t} = -\nabla p^{\mathrm{k}} + \rho^{\mathrm{k}} v^{\mathrm{k}}(R^{\mathrm{k}}_{\mathrm{rea}} + Q^{\mathrm{k}}_{\mathrm{b}}) - 12\mu^{\mathrm{k}}\left(\frac{1}{(l^{\mathrm{k}}_{\mathrm{d,g}})^2} + \frac{1}{(w^{\mathrm{k}}_{\mathrm{C}})^2}\right) v^{\mathrm{k}} \tag{28}$$

where p is the pressure, μ the gas viscosity, w_{C} the width of a gas channel and the operator D/Dt is substantial time derivative that is shown by the following equation:

$$\frac{\mathrm{D}v^{\mathrm{k}}}{\mathrm{D}t} = \frac{\partial v^{\mathrm{k}}}{\partial t} + v^{\mathrm{k}}\frac{\partial v^{\mathrm{k}}}{\partial x} \tag{29}$$

The viscous term in Eq. (28) is derived from the Hele–Show model. This term includes the effect of viscous drags between two pairs of facing walls in a channel.

The equation of chemical species j is shown by the following equation:

$$\frac{\mathrm{D}C^{\mathrm{k}}_j}{\mathrm{D}t} = -\frac{r^{\mathrm{k}}_j}{l^{\mathrm{k}}_{\mathrm{d,g}}} + C^{\mathrm{k}}_j(R^{\mathrm{k}}_{\mathrm{rea}} + Q^{\mathrm{k}}_{\mathrm{b}}) + \sum_n C^{\mathrm{k}}_{j(n)} Q^{\mathrm{k}}_{\mathrm{b}(n,\mathrm{in})} - \sum_n C^{\mathrm{k}}_j Q^{\mathrm{k}}_{\mathrm{b}(n,\mathrm{out})} \tag{30}$$

where C_j is concentration of a chemical species j, $C_{j(n)}$ the concentration of a chemical species j at the next channel to the n direction, $Q_{\mathrm{b}(n,\mathrm{in})}$ the gas flow rate through GDL from the n direction adjoining channel to this point and $Q_{\mathrm{b}(n,\mathrm{out})}$ is gas flow rate through GDL from this point to the n direction adjoining channel. The equations of species were derived to eight kinds of chemical species: $C^{\mathrm{a}}_{\mathrm{H_2}}$, $C^{\mathrm{a}}_{\mathrm{N_2}}$, $C^{\mathrm{a}}_{\mathrm{H_2O(v)}}$, $C^{\mathrm{a}}_{\mathrm{H_2O(l)}}$, $C^{\mathrm{c}}_{\mathrm{O_2}}$, $C^{\mathrm{c}}_{\mathrm{N_2}}$, $C^{\mathrm{c}}_{\mathrm{H_2O(v)}}$, $C^{\mathrm{c}}_{\mathrm{H_2O(l)}}$ that are hydrogen, oxygen, nitrogen, vapor and condensed water in anode and cathode channel.

The equations of energy are shown by the following equations:

$$\text{(Gas)}\quad \frac{\mathrm{D}T^{\mathrm{k}}}{\mathrm{D}t} = \frac{q_1^{\mathrm{k}} + q_2^{\mathrm{k}}}{\rho^{\mathrm{k}} C_{\mathrm{p}}^{\mathrm{k}} l_{\mathrm{d,g}}^{\mathrm{k}}} + T^{\mathrm{k}}(R_{\mathrm{rea}}^{\mathrm{k}} + Q_{\mathrm{b}}^{\mathrm{k}}) + \sum_n T_n^{\mathrm{k}} Q_{\mathrm{b}(n,\mathrm{in})}^{\mathrm{k}} - \sum_n T^{\mathrm{k}} Q_{\mathrm{b}(n,\mathrm{out})}^{\mathrm{k}} \quad (31)$$

$$\text{(Solid)}\quad \rho^{\mathrm{s}} C_{\mathrm{p}}^{\mathrm{s}} \frac{\partial T^{\mathrm{s}}}{\partial t} = k^{\mathrm{s}} \nabla^2 T^{\mathrm{s}} + \frac{q_3^{\mathrm{s}} + q_4^{\mathrm{s}} + q_5^{\mathrm{s}} + q_6^{\mathrm{s}}}{l^{\mathrm{s}}} \quad (32)$$

In the energy equation of gas, C_{p} is the specific heat, T the temperature and q_1 and q_2 are heat fluxes from a solid phase and a back plate, respectively. T_n is the gas temperature in the next channel to the n direction. In the equation of a solid phase, k is the heat conductivity, l^{s} the thickness of solid phase, q_3 the heat value per unit area as a result of electrochemical reaction, q_4 and q_5 the heat fluxes from gas and a back plate, respectively, q_6 the latent heat flux of water condensation and the superscript 's' is a solid phase. These heat flux and heating value are shown by the following equations:

$$\begin{aligned} q_1^{\mathrm{k}} &= h^{\mathrm{k}}(T^{\mathrm{s}} - T^{\mathrm{k}}) \\ q_2^{\mathrm{k}} &= U_{\mathrm{T}}^{\mathrm{k}}(T^{\mathrm{b}} - T^{\mathrm{k}}) \\ q_3^{\mathrm{s}} &= (E_{\Delta H} - V)i \\ q_4^{\mathrm{s}} &= h^{\mathrm{a}}(T^{\mathrm{a}} - T^{\mathrm{s}}) + h^{\mathrm{c}}(T^{\mathrm{c}} - T^{\mathrm{s}}) \\ q_5^{\mathrm{s}} &= U_{\mathrm{T}}^{\mathrm{s(a)}}(T^{\mathrm{b}} - T^{\mathrm{s}}) + U_{\mathrm{T}}^{\mathrm{s(c)}}(T^{\mathrm{b}} - T^{\mathrm{s}}) \\ q_6^{\mathrm{s}} &= -\Delta H_{\mathrm{H_2O}}(r_{\mathrm{H_2O(l)}}^{\mathrm{a}} + r_{\mathrm{H_2O(l)}}^{\mathrm{c}}) \end{aligned} \quad (33)$$

where h is heat transfer coefficient of anode or cathode gas, $E_{\Delta H}$ the value when the change of water enthalpy was converted to voltage, V the voltage, i the current density, $\Delta H_{\mathrm{H_2O}}$ the change of water enthalpy between vapor and liquid, $U_{\mathrm{T}}^{\mathrm{k}}$ the overall heat transfer coefficient between anode gas or cathode gas and a back plate and $U_{\mathrm{T}}^{\mathrm{s(k)}}$ is the overall heat transfer coefficient between anode or cathode side back plate and solid phase. These overall heat transfer coefficients are shown by the following equations:

$$\begin{aligned} U_{\mathrm{T}}^{\mathrm{k}} &= \frac{1}{\dfrac{1}{h^{\mathrm{k}}} + \dfrac{l^{\mathrm{sep}}}{k^{\mathrm{sep}}}} \\ U_{\mathrm{T}}^{\mathrm{s(k)}} &= \frac{k^{\mathrm{sep}}}{l^{\mathrm{sep}} + l_{\mathrm{d,g}}^{\mathrm{k}}} \end{aligned} \quad (34)$$

where l^{sep} is the separator thickness between a back plate and a gas phase and k^{sep} is the heat conductivity of a separator.

Reaction and condensation rates of each ingredient are shown by the following equations:

$$\begin{aligned} r_{\mathrm{H_2}}^{\mathrm{a}} &= \frac{i}{2F} \\ r_{\mathrm{H_2O(v)}}^{\mathrm{a}} &= \alpha\frac{i}{F} + l_{\mathrm{d,g}}^{\mathrm{a}} b_{\mathrm{c}} \left(C_{\mathrm{H_2O}(v)}^{\mathrm{a}} - \frac{P_{\mathrm{H_2O,sat}}^{\mathrm{a}}}{RT^{a}} \right) \\ r_{\mathrm{N_2}}^{\mathrm{a}} &= 0 \\ r_{\mathrm{H_2O(l)}}^{\mathrm{a}} &= -l_{\mathrm{d,g}}^{\mathrm{a}} b_{\mathrm{c}} \left(C_{\mathrm{H_2O(v)}}^{\mathrm{a}} - \frac{P_{\mathrm{H_2O,sat}}^{\mathrm{a}}}{RT^{\mathrm{a}}} \right) \\ r_{\mathrm{O_2}}^{\mathrm{c}} &= \frac{i}{4F} \\ r_{\mathrm{H_2O(v)}}^{\mathrm{c}} &= -(1+2\alpha)\frac{i}{2F} + l_{\mathrm{d,g}}^{\mathrm{c}} b_{\mathrm{c}} \left(C_{\mathrm{H_2O(v)}}^{\mathrm{c}} - \frac{P_{\mathrm{H_2O,sat}}^{\mathrm{c}}}{RT^{\mathrm{c}}} \right) \\ r_{\mathrm{N_2}}^{\mathrm{c}} &= 0 \\ r_{\mathrm{H_2O(l)}}^{\mathrm{c}} &= -l_{\mathrm{d,g}}^{\mathrm{c}} b_{\mathrm{c}} \left(C_{\mathrm{H_2O(v)}}^{\mathrm{c}} - \frac{P_{\mathrm{H_2O,sat}}^{\mathrm{c}}}{RT^{\mathrm{c}}} \right) \end{aligned} \quad (35)$$

where F is the Faraday's constant, R the gas constant, $P_{\mathrm{H_2O,sat}}$ the saturated vapor pressure, α the water transfer coefficient and b_{c} is the condensation rate constant.

Gas flow rate through GDL is calculated by the following Darcy's model:

$$Q_{\mathrm{b}(n)}^{\mathrm{k}} = \frac{k_{\mathrm{p}}}{\mu^{\mathrm{k}}} \frac{l_{\mathrm{GDL}}^{\mathrm{k}}}{l_{\mathrm{d,g}}^{\mathrm{k}} w_{\mathrm{C}}^{\mathrm{k}} w_{\mathrm{L}}^{\mathrm{k}}} (p^{\mathrm{k}} - p_n^{\mathrm{k}}) \quad (36)$$

where k_{p} is the permeability of GDL, l_{GDL} the thickness of GDL and w_{L} is the width of the land area that is between channels.

Current density i was calculated with Eqs. (6) and (24). In this model, current density was calculated by the following equation as the function of local concentration and temperature:

$$i = f(V, C_{\mathrm{H_2O(v)}}^{\mathrm{a}}, C_{\mathrm{O_2}}^{\mathrm{c}}, p_{\mathrm{sat}}^{\mathrm{a}}, T^{\mathrm{s}}) \quad (37)$$

It is thought that water is moved under two mechanisms, electro-osmosis and back diffusion in an electrolyte membrane. When one proton moves from the anode side to the cathode side, the water movement coefficient α shows the net number of water molecules moving along with proton. This is from the method by Nguyen and White [5].

The local concentration, temperature, flow velocity and current density were calculated with Eqs. (25)–(37). Their partial differential equations are discretized by the finite differential method. The boundary conditions of flow velocity, temperature and concentration are set as followings:

(1) *The gas inlet boundary*: these variables are constant.
(2) *The gas outlet boundary*: the gradients of these variables are constant.

Current density and water transfer coefficient were calculated all over the electrode area. Those variables were calculated until becoming stationary state. The relative errors

of balance equation of mass, species and energy became less than 1% in all the calculations.

3. Results and discussions

3.1. Relationship between gas flow rate and pressure drop with or without GDL

In order to confirm the validity of this numerical analysis model including gas flow through GDL, the cathode gas flow rate and pressure drop were measured in a 25 cm^2 cell with or without GDL under the condition without reactions, and calculation results were compared with the experimental results. Fig. 12 shows the gas channel shape of a separator in flow experiments without reactions. Fig. 12a is a serpentine channel separator with 1 channel, (b) is a serpentine channel separator with 5 channels, (c) is a parallel channel separator with 25 channels and (d) is a semi-serpentine channel separator with 8 channels. Width and depth of the channel were both 1 mm, width of the land area was also 1 mm in each separator, and thickness of GDL was 300 μm. The supplied gas was not humidified, and cell and gas temperature were 25 °C. The value of permeability of GDL was treated as 2.5×10^{-11} m^2 for the numerical analysis.

Fig. 13 shows the relationship between gas flow rate and pressure drop in the cathode side of a 25 cm^2 cell by the experiment and the calculation with each separator. The influence of gas flow through GDL was examined with four kinds of separator for the experiment and the calculation. However, as this analysis model developed in this study was derived from assuming that each channel did not branch off or confluent between the inlet and the outlet, the experimental results could not be compared with calculation results in Fig. 13c

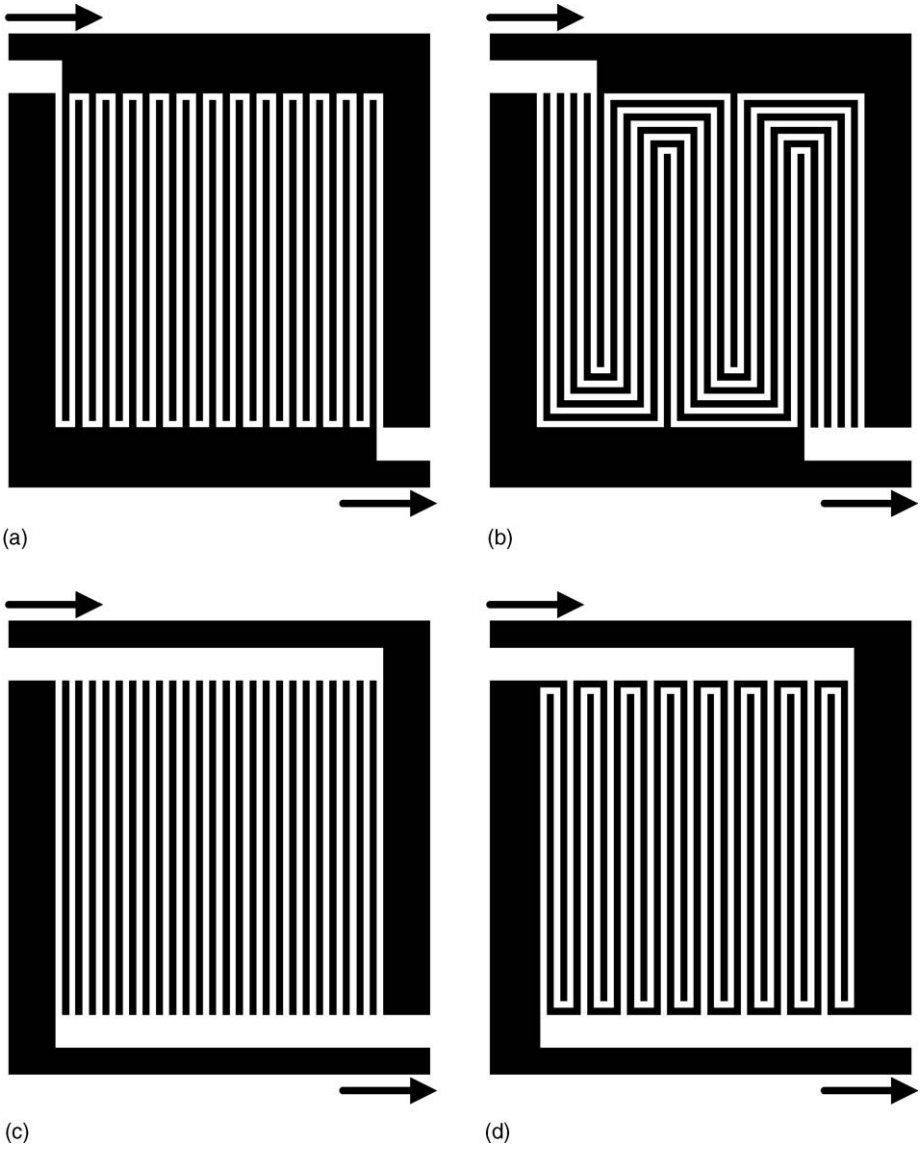

Fig. 12. (a–d) Gas channel shape of separator in non-reaction flow experiments.

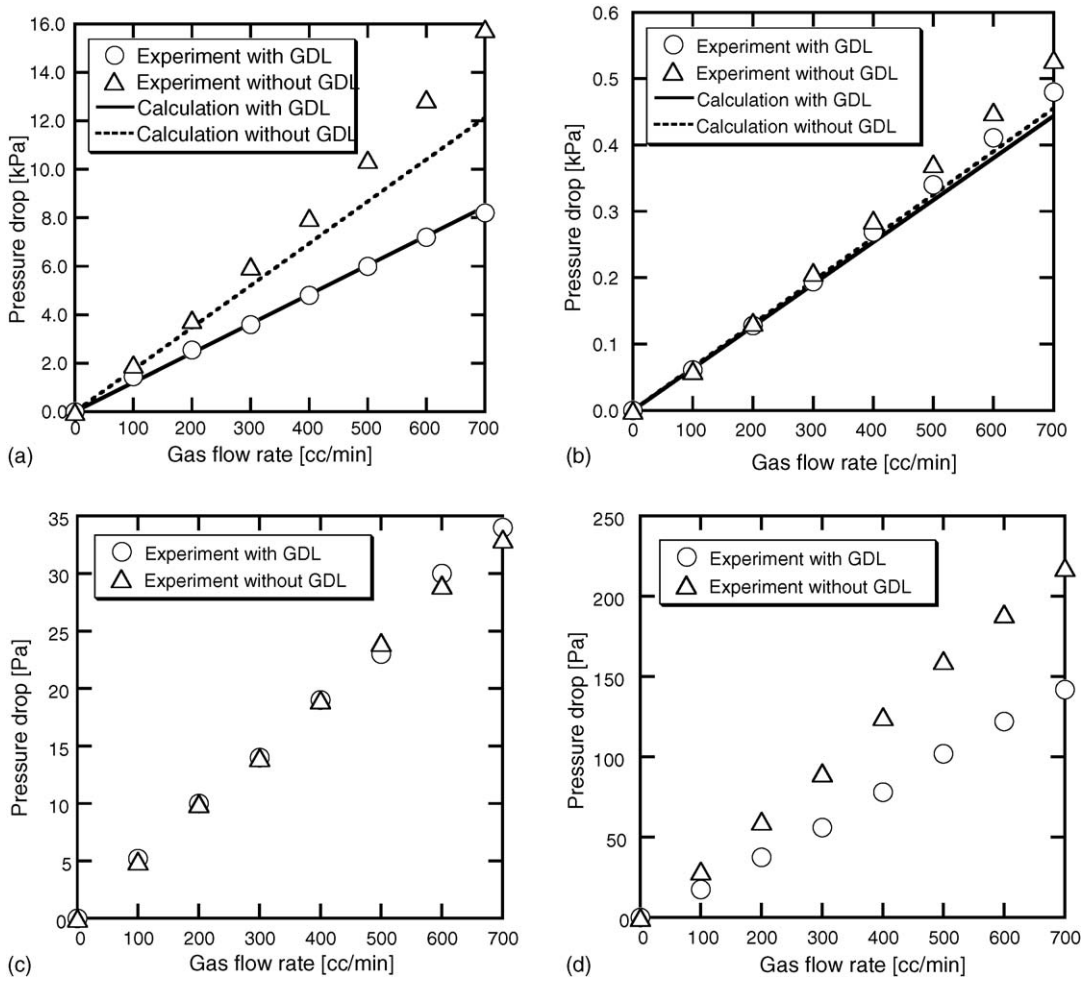

Fig. 13. Relationship between gas flow rate and pressure drop in cathode side of 25 cm^2 cell by experiment and calculation: (a) serpentine separator with one channel; (b) serpentine separator with five channel; (c) parallel separator; (d) semi-serpentine separator.

and d. In Fig. 13a and c, it was found that the influence of GDL on pressure drop was large in the case of serpentine separator with one channel and semi-serpentine separator. And pressure drop in the experiments without GDL was 1.5 times as large as that with GDL. On the other hand, in Fig. 13b and d, the difference of pressure drop between the experiments with GDL and that without GDL was small. It was considered that the differential pressure between adjoining channels of serpentine separator with one channel and semi-serpentine separator was larger than that of other separators. The gas flow rate through GDL was increased by its differential pressure, and the gas flow along the channel became incomplete. Consequently, the actual PEFC is sure to have GDL, which occurs non-uniform flow, and such flow condition is different by separator shapes.

Next, the calculation results were compared with experimental results in Fig. 13a and b. The pressure drop was theoretically in proportion to gas flow rate when the gas flow condition was laminar flow. However, as the gas flow rate per channel was high in the case of one channel separator, the gas flow condition became turbulence flow without GDL. And pressure drop of the experiment was not in proportion to the gas flow rate, as a result, there was a small difference between the experiment results and calculation results without GDL in one channel serpentine separator (Fig. 13a). In other condition, the calculation results by this model were almost equal to the experimental results, and the validity of this model including such gas flow through GDL was confirmed.

3.2. *Effect of channel depth on output performance and current density distribution*

Fig. 14 shows the separator shape of the anode side and the cathode side that is the target in this study. The electrode area was 150 mm^2. The width of channel and land was both 1 mm, and the number of channels was 15. Fig. 15 shows the developed view of a single cell and gas flow pattern with the separator of Fig. 14. As the same separators were put together like Fig. 15a, gas flow pattern are shown in Fig. 15b. Table 2 shows the calculation parameter including the operating condition and the dimensions of MEA, GDL and separator. It was supposed that physical properties were constant, because the effect of changing gas composition in a cell on physical prop-

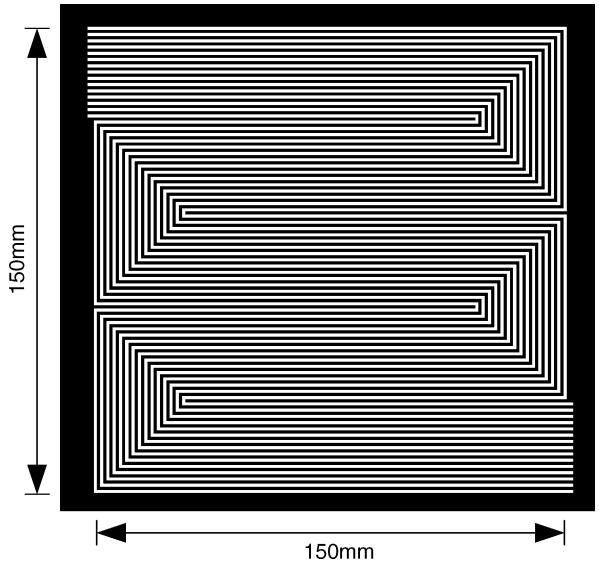

Fig. 14. Gas channel shape of separator in 225 cm^2 cell calculation.

erties was little. GDL effective porosity was 0.2 as reference value, and the effect of liquid water in GDL was included in analysis model indirectly. And it was supposed that the channel depth of anode and cathode equaled each other. In order to examine the characteristic of current density–cell voltage in each condition, the calculation was carried out from 0.9 V to 0.05 V by the 0.05 V steps, and it took 8 h per one calculation condition by Penitum4® 3.2 GHz PC.

The effect of the channel depth was examined with the numerical analysis model developed in this study. Fig. 16 shows the current density–cell voltage curve of each channel depth. In this graph, it was found that the cell voltage of a shallow channel was higher than that of a deep channel at high current density condition. The reason was that the differential pressure between adjoining channels increased in the case of the shallow channel, and that the oxygen transfer rate

Table 2
Calculation condition of PEFC actual size cell analysis

Pressure (MPa)	0.1
Inlet gas and humidify temperature (°C)	60
Back plate temperature (°C)	60
Inlet gas composition	
Anode	Pure H_2
Cathode	Air (O_2:N_2 = 21:79)
Inlet gas flow rate ($m^3\ s^{-1}$)	
Anode	16.67×10^{-5}
Cathode	25.00×10^{-5}
Thickness of membrane (μm)	30
Size of catalyst layer (cm^2)	225
GDL thickness (μm)	300
GDL permeability (m^2)	2.5×10^{-11}
Number of the channel	15
Channel width (mm)	1
Shoulder width (mm)	1
Channel depth (mm)	0.5, 1.0, 1.5

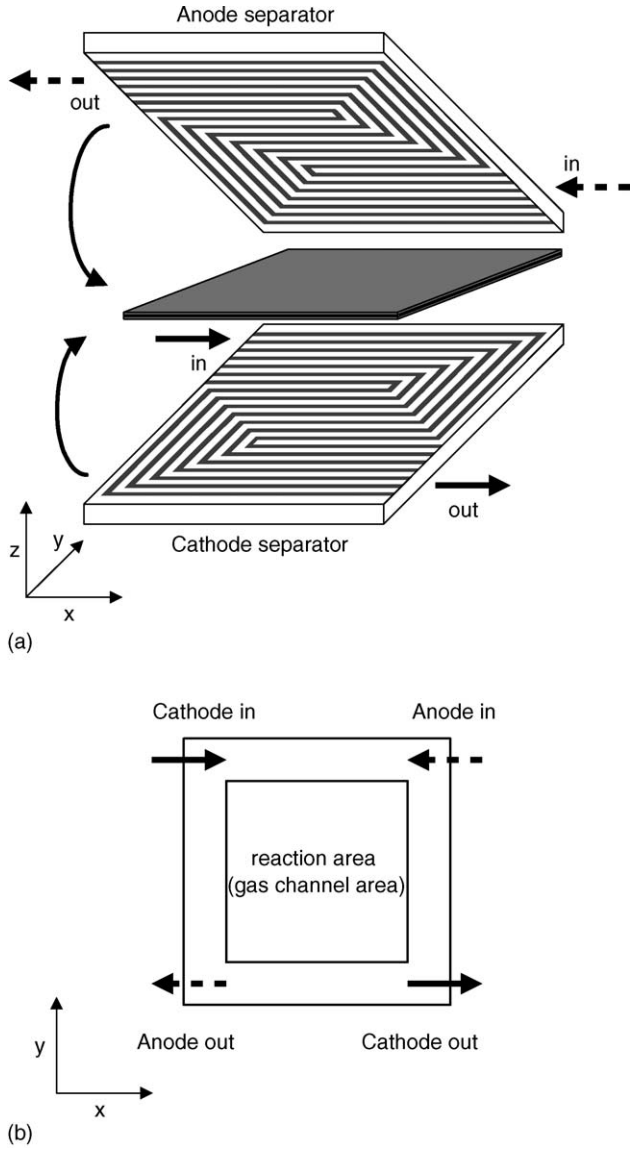

Fig. 15. Developed view of single cell (a) and gas flow pattern (b) (viewpoint of (b): from back to anode separator).

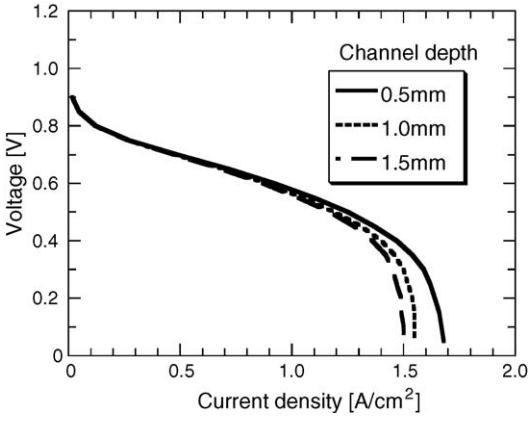

Fig. 16. Effect of channel depth on current density–voltage curve.

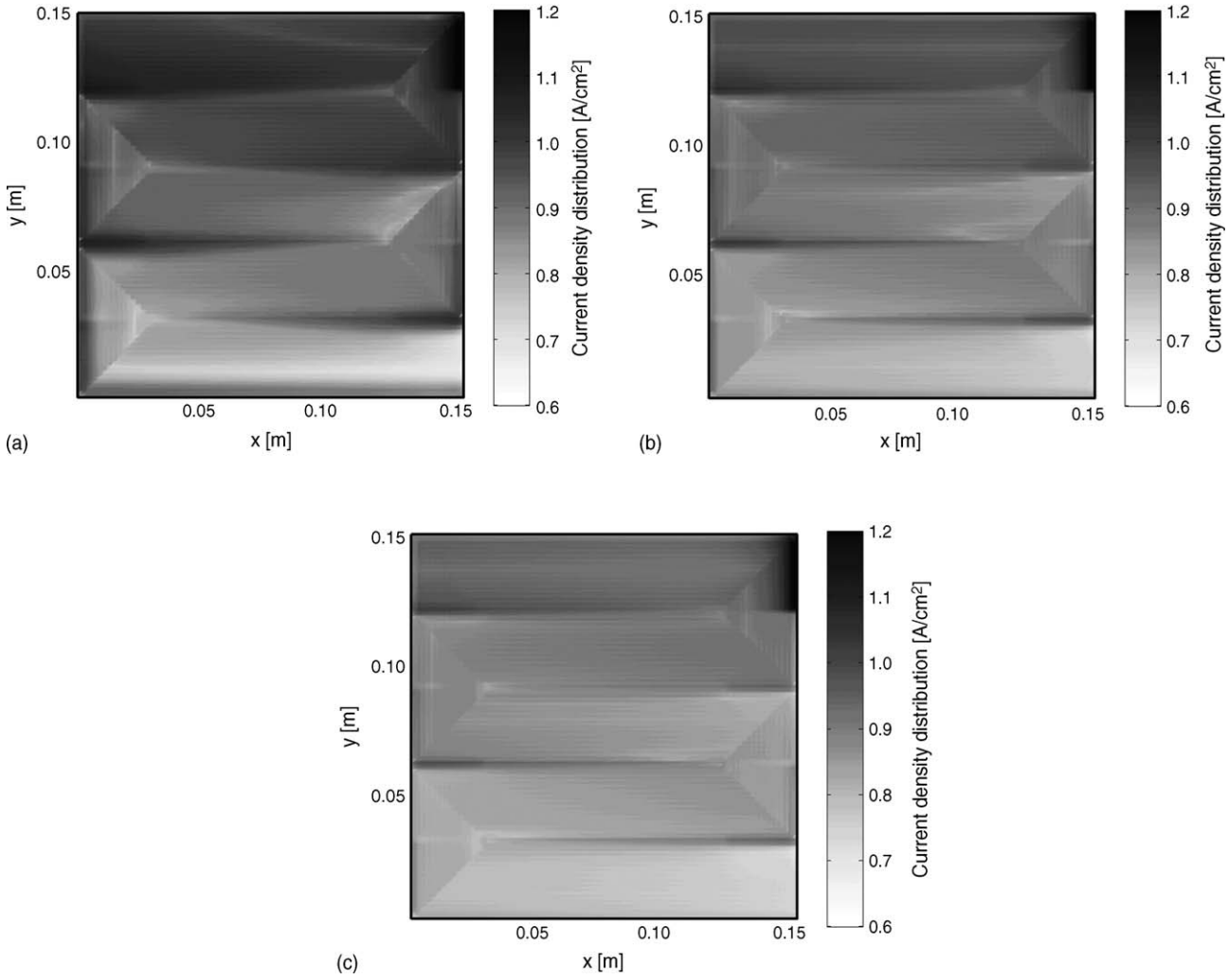

Fig. 17. Influence of channel depth on current density distribution. Channel depth: (a) 0.5 mm; (b) 1.0 mm; (c) 1.5 mm.

to electrode was increased by the gas flow through GDL. In this study, the anode channel depth was also changed, however, as the hydrogen concentration overvoltage was ignored, the gas flow through anode GDL did not affect the reaction rate directly. And as the anode gas of about 100% in relative humidity flowed in cell, anode relative humidity which affect local ionic conductivity of membrane became almost uniform even if anode gas flow rate distribution became remarkable by the gas flow through GDL. Consequently, the effect of cathode channel depth on cell performance was larger than that of anode channel depth under this operating condition. Fig. 17 shows the current density distribution of each channel depth at 0.6 V. In this graph, the current density was the highest at the turning point of channel under all conditions, and tendency of 0.5 mm channel depth was larger than other conditions. However, there were the parts of low current density at the downstream area. The reason was that the gas did not flow uniformly through GDL. It is considered that the non-uniform current density distribution may cause the non-uniform water content and temperature distribution of electrolyte membrane, and that it may reduce the durability of a cell. On the other hand, the concept of reduction of channel depth in order to increase the oxygen transfer rate to electrode is equal to that of the interdigitated channel proposed by Nguyen [14]. However, the power of supplying gas must be considered to examine the effectiveness such separator shape. Because the net generated power is different between the generated electric power and the power of supplying. From these viewpoints, uniformity of current density and pressure drop of each channel depth were compared. Fig. 18 shows the effect of channel depth on the rate of the maximum current density to the minimum current density and pressure drop at 0.6 V. As channel depth is smaller, the ratio of current density is larger in Fig. 18a, and the pressure drop is larger in Fig. 18b. The pressure drop of the 0.5 mm depth was four times as much as that of the 1.0 mm depth.

In order to examine the optimal separator shape, the performance of oxygen transfer to electrode and the pressure drop must be evaluated comprehensively, in addition to mechanical strength, manufacturing cost and the performance of conductivity. Furthermore, the performance of removing liquid water in a channel must be evaluated. In

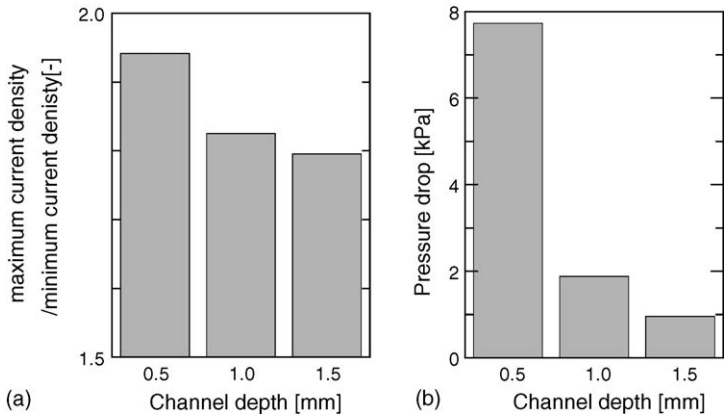

Fig. 18. (a and b) Effect of channel depth on the rate of maximum current density to minimum current density and pressure drop at 0.6 V.

the case of deep channel, it is expected that the performance of removing liquid water decreases. About this point, this numerical analysis model must be improved to examine this.

4. Conclusion

In order to calculate an actual scale cell of PEFC including gas flow through GDL, the effect of gas flow rate through GDL was examined by the numerical analysis, and the oxygen transfer model was made with the theoretical model. Next, this oxygen transfer model was combined with the thermal flow analysis model, and PEFC reaction and flow analysis model of an actual size was made. Furthermore, depth of separator channel was evaluated with this model from the viewpoint of the characteristic of current density and voltage, current density distribution and pressure drop. The validity of this model was confirmed by experiments. The following results were obtained by these examinations:

1. The oxygen mass transfer rate could be shown as the function of the Reynolds number and the Schmidt number. And the rate was in promotion of the square root of the Reynolds number.
2. The experiments without reactions showed that the effect of gas flow through GDL on the whole flow condition was large when the differential pressure between adjoining channels was large.
3. The numerical analysis showed the output density increased as depth of separator channel was smaller. However, the pressure drop and current density distribution increased, too.
4. The current density at the turning point of a separator channel was the highest in the whole electrode area under each condition.

The numerical analysis developed in this study is a very simple model with the oxygen transfer model and the one-dimension flow model in gas channel. It does not suit to examine the microscopic phenomena, however the macroscopic phenomena can be examined, and this model can be applied to design of the PEFC system. On the other hand, GDL effective porosity was used as a parameter including the effect of liquid water. However, it is not advisable to decide the GDL effective porosity by fitting with experimental results under various conditions, and it is impossible to examine liquid water distribution locally in GDL from this method. Therefore, development of a detailed liquid water model is needed. And the current density distribution was calculated with the approximate model of oxygen transfer in cathode GDL, which was developed with the calculation results based on the assumption to ignore the concentration diffusion between adjoining channels. (The concentration of channels was set to be equal to each other.) For example, in the case of the turning point of a channel, there is relation between the upstream and the downstream in the same channel, so the concentration of the downstream channel is lower than that of the upstream channel by electrochemical reaction, therefore it is necessary to consider the difference of concentration. In our future study, it is expected that this model will be improved to apply the various conditions including the influence of liquid water and various concentration conditions in order to examine the current density distribution strictly in an actual cell.

Acknowledgement

This research was partially supported by the research and development of polymer electrolyte fuel cell from the New Energy and Industrial Technology Development Organization (NEDO), Japan.

References

[1] D.M. Bernardi, M.W. Verbrugge, Mathematical model of a gas diffusion electrode bonded to a polymer electrolyte, AIChE J. 37 (8) (1992) 1151–1163.
[2] D.M. Bernaldi, M.W. Verbrugge, A mathematical model of the solid–polymer–electrolyte fuel cell, J. Electrochem. Soc. 139 (9) (1992) 2477–2491.

[3] T.E. Springer, T.A. Zawodzinski, S. Gottesfeld, Polymer electrolyte fuel cell model, J. Electrochem. Soc. 138 (8) (1991) 2334–2342.
[4] T.F. Fuller, J. Newman, Water and thermal management in solid–polymer–electrolyte fuel cells, J. Electrochem. Soc. 140 (5) (1993) 1218–1225.
[5] T.V. Nguyen, R.E. White, A water and heat management model for proton-exchange-membrane fuel cells, J. Electrochem. Soc. 140 (8) (1993) 2178–2186.
[6] J.S. Yi, T.V. Nguyen, An along-the-channel model for proton exchange membrane fuel cells, J. Electrochem. Soc. 145 (4) (1998) 1149–1159.
[7] S. Um, C.Y. Wang, K.S. Chen, Computational fluid dynamics modeling of proton exchange membrane fuel cells, J. Electrochem. Soc. 147 (12) (2000) 4485–4493.
[8] Z.H. Wang, C.Y. Wang, K.S. Chen, Two-phase flow and transport in the air cathode of proton exchange membrane fuel cells, J. Power Sources 94 (2001) 40–50.
[9] S. Dutta, S. Shimpalee, J.W. Van Zee, Three-dimensional numerical simulation of straight channel PEM fuel cells, J. Appl. Electrochem. 30 (2000) 135–146.
[10] T. Berning, D. Lu, N. Djilali, Three-dimensional computational analysis of transport phenomena in a PEM fuel cell, J. Power Sources 106 (2002) 284–294.
[11] S. Mazumder, J.V. Cole, Rigorous 3-D mathematical modeling of PEM fuel cells model predictions with liquid water transport, J. Electrochem. 150 (11) (2003) 1510–1517.
[12] P.-W. Li, L. Schaefer, Q.-M. Wang, T. Zhang, M.K. Chyu, Multi-gas transportation and electrochemical performance of a polymer electrolyte fuel cell with complex flow channels, J. Power Sources 115 (2003) 90–100.
[13] T. Berning, N. Djilali, Three-dimensional computational analysis of transport phenomena in a PEM fuel cell—a parametric study, J. Power Sources 124 (2003) 440–452.
[14] T.V. Nguyen, A gas distributor for proton-exchange-membrane fuel cells, J. Electrochem. Soc. 143 (1996) L103.
[15] S. Um, C.Y. Wang, Three-dimensional analysis of transport and electrochemical reactions in polymer electrolyte fuel cells, J. Power Sources 125 (2004) 40–51.
[16] H. Dohle, R. Jung, N. Kimiaie, J. Mergel, M. Müller, Interaction between the diffusion layer and the flow field of polymer electrolyte fuel cells—experiments and simulation studies, J. Power Sources 124 (2003) 371–384.
[17] P.H. Oosthuizen, L. Sun, K.B. McAuley, The effect of channel-to-channel gas crossover on the pressure and temperature distribution in PEM fuel cell flow plates, Appl. Therm. Eng. 25 (2005) 1083–1096.
[18] G. Inoue, Y. Matsukuma, M. Minemoto, Evaluation of the optimal separator shape with reaction and flow analysis of polymer electrolyte fuel cell, J. Power Sources 154 (2006) 18–34.
[19] G. Inoue, Y. Matsukuma, M. Minemoto, Evaluation of the thickness of membrane and gas diffusion layer with simplified two-dimensional reaction and flow analysis of polymer electrolyte fuel cell, J. Power Sources 154 (2006) 8–17.
[20] R.B. Bird, W. Steward, E.N. Lightfood, Transport Phenomena, Wiley, New York, 1960.